



Broadband circularly polarized dielectric resonator antenna for UWB applications

SACHIN KUMAR YADAV*^{ID}, AMANPREET KAUR and RAJESH KHANNA

Electronics and Communication Engineering Department, Thapar Institute of Engineering and Technology, Patiala, India
e-mail: yadav_sachinyadav@yahoo.com; amanpreet.kaur@thapar.edu; rkhananna@thapar.edu

MS received 19 January 2021; revised 21 January 2022; accepted 27 January 2022

Abstract. In this paper, a compact circularly polarized asymmetric dielectric resonator antenna (DRA) excited by a quarter-wave transformer (QWT) feedline is proposed for ultra-wideband (UWB) applications. The DRA consists of two rectangular ceramic blocks with the same permittivity ($\epsilon_{DR} = 9.8$) and an F-shaped metallic strip combined with the partial ground. The proposed antenna is supported first and third-order modes as $TE_{\delta 11}$ and $TE_{\delta 13}$ at 9.1 and 11.28 GHz. The proposed antenna covers ultra-wideband (UWB) range from 6.4 to 12.4 GHz (impedance bandwidth of 63.8 %) with a peak gain of 6.01 dBi at 11.5 GHz. The broad AR bandwidth of the proposed antenna is achieved by the asymmetric structure of DR and the modified ground. The simulated AR bandwidth (≤ 3 dB) of the proposed antenna is 63.8% (6.4 to 12.4 GHz), and the measured AR bandwidth is 2.5% (5.8 to 6.1 GHz) and 43.7% (6.9 to 10.9 GHz). The proposed antenna can be used for C, X band applications.

Keywords. Circular polarization; asymmetric DRA; rectangular DRA; ultra-wideband; quarter wave transformer.

1. Introduction

Ultra-wideband (UWB) devices use narrow or short-duration pulses, making massive or wideband transmission data transfer possible. UWB innovation holds a good agreement for an enormous range of new applications. It accepts unique advantages to organizations and buyers. It can work by using the capacity that involves existing radio services without interference, allowing the proficient use of range assets [1]. The compact antenna for the UWB range communication system has achieved convenience attention in industrial and academic communities. Due to the high data transmission and reception processing rate, simple hardware configuration, low power consumption, and low-cost design, the dielectric resonator antenna (DRA) is preferred. UWB antennas are essential in many systems, including electronic warfare, radar, medical imaging, and wireless communication. Several DRA has been studied to date, which vary structural designs [2, 3]. DRA has attained agreeable consideration for designing the UWB antenna due to its remarkable features [4–7] indicated by the previous work of Majeed on UWB from 6.6 GHz to 11.3 GHz [8].

The main noticeable features of dielectric resonator (DR) antennas (DRAs) have low metallic losses, wide

bandwidth, lightweight, and high radiation efficiency [9, 10]. Short-range communication faces a rich scattering environment, which gives problems like fading due to the multipath and power loss due to disintegrating conditions or mismatch of the transmitter and receiver antenna. DRA has various techniques to achieve CP, including the modification of the shape of DR [11–13], metallic strips [14], Cross-slot-coupled [15], and single/dual feeding structure [16, 17]. With a 3 dB axial ratio (AR) bandwidth, an ultra-wideband DRA is used as circular polarised (CP) for wireless applications [18]. In some methods, the CP depends on the structure of the DR. Therefore, the DRA shape is modified to be as asymmetric (width and height) structure for the broadband CP response in the UWB region.

A compact asymmetrical structured DRA with an F-shaped metallic strip in the ground plane is used to achieve wider AR bandwidth (3-dB) for the UWB operations. The proposed antenna structure is designed, analyzed, and optimized using CST microwave studio software. The reflection coefficient of the proposed antenna is measured using a KEYSIGHT (E5063A) vector network analyzer, and the far-field results of the antenna are obtained by the anechoic chamber. The present work is organized as follows: Section 2 presents the proposed antenna geometry and configuration. Section 3 describes the parametric optimization to achieve the desired result. Section 4

*For correspondence

presents simulated and measured results. The conclusion for the proposed antenna is presented in section 5.

2. Antenna geometry and configuration

The geometry of the circularly polarized asymmetrical DRA is shown in figure 1. It consists of two rectangular blocks, having the same permittivity $\epsilon_{DR} = 9.8$. These blocks are called dielectric resonators (DRs), first and second block height, length, width are t_{dr1} , t_{dr2} , l_{dr1} , l_{dr2} , w_{dr1} , w_{dr2} , respectively, as shown in figures 1 (a) and (b). The complete design is printed on a low-cost FR4 substrate with a permittivity $\epsilon_s = 4.4$ with dimensions ($L_s \times W_s \times t_s$) as $25 \times 25 \times 0.8 \text{ mm}^3$. On top of this substrate, a microstrip feedline is printed to excite the DR radiator with 50Ω input impedance. The feeding network ensures proper impedance matching in a wide range of frequencies. The microstrip feed-line have two parts $l_{f1} \times w_{f1}$ (50Ω) and l_{f2} ($\lambda/4$) $\times w_{f2}$, which are added to each other. The metallic F-shaped strip added with a partial ground plane is printed on the bottom side of the substrate. The partial ground plane has dimensions $L_g \times W_g$, and F-shape metallic strip dimensions are l_{t1} , l_{t2} , l_{t3} , s_{t1} , s_{t2} , as shown in figures 1 (a and b). The metallic strips are used in DRA to improve overall gain and AR bandwidth [15, 16]. The perspective and side view of the antenna are shown in figures 1(c)–(d). All design parameters with optimized values are given in Table 1.

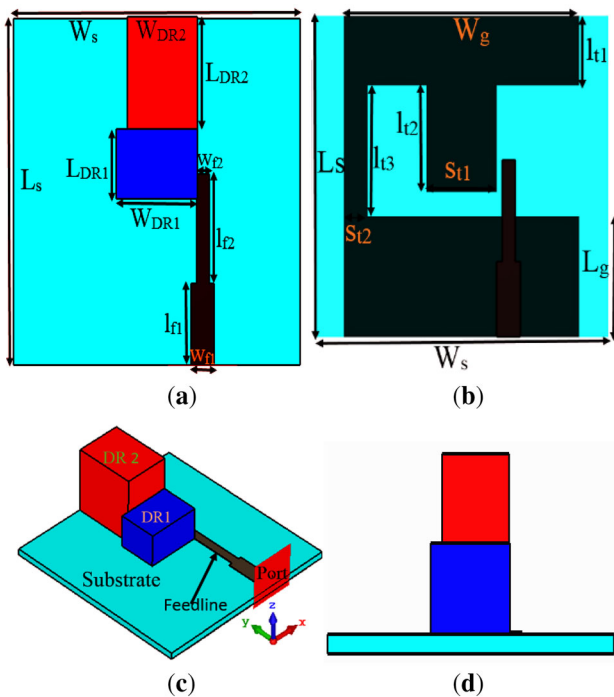


Figure 1. Compact CPDRA (a) Front view, (b) Back view, (c) Perspective and (d) Side view.

2.1 Antenna operation

The complete evolution of the final antenna (Ant. 5) is shown in five different stages as Ant.1, Ant.2, Ant.3, Ant.4, and Ant.5, respectively, shown in figure 2. All antennas except Ant. 1 can be employed for wideband applications, as shown in figure 3(a). In the second stage (Ant. 2), DR and the partial ground plane achieve the wide impedance bandwidth (70.3%) but not reported 3-dB AR bandwidth. In the third stage (Ant. 3), an F-shaped metallic strip is added with the partial ground, which enhanced the peak gain from 3.7 dB to 5.3 dB, as observed in figure 3(b). In the fourth stage (Ant. 4), a second block (Red) is placed above the initial block (the pink), which gave two different sections with height 4 mm (DR1) and 8 mm (DR2) to achieve the 3-AR bandwidth of 17.4%. In the final stage (Ant. 5), the width of the DR1 is increased to achieve 3-dB AR bandwidth of 63.8%, as observed in figure 3(c). Table 2 shows the performance of the designed antenna by five different stages.

2.2 Widen bandwidth mechanism

The broad bandwidth mechanism is discussed in this section using the current distribution on the metallic surface and the DR perturbation theory. Firstly, the current distribution of the antenna is presented in figures 4a–d. The current rotation is observed from the surface current distribution on the full, with DGS and partial ground plane, as shown in figure 4. Also, it can be observed that the decoupling structure provided the maximum surface current on the edges of the decoupling slot with different frequencies. The current distribution is shown in figures 4(a)–(b) at 7.2 GHz with single resonance path. Figures 4c–d offers the current cancellation having two resonance paths at 9 GHz. As compare to full ground, the modified ground is reported good impedance bandwidth, as shown in figures 4(b) and (d).

Secondly, perturbation theory is employed in DR asymmetrical structure to improve the impedance and AR bandwidth of the antenna. Two DRs are taken, and calculate the volume (V_{dra}) of DR1 and DR2 are 140 and 384 (total = 524) mm^3 , as shown in figure 1c. The total volume (V_{total}) of DRA is 728 mm^3 ($13 \times 7 \times 8$). So air-spaced volume $V_s = 728 - 524 = 204 \text{ mm}^3$. The effective permittivity (ϵ_{reff}) of the DR depends on the volume (V_s , V_{dra}) and $\epsilon_{DR} = 10.2$. With and without perturbation, DR is shown in figure 2. So calculated $\epsilon_{reff} = 7.14$ from (1) and quality factor Q and Q_p are 2.1 and 1.79 using Eqs. (2)–(3). Thus, as the ϵ_{reff} and Q_p of DR decreases vice versa, bandwidth of antenna is improved.

$$\epsilon_{reff} = \frac{\epsilon_{DR} V_{dra} + \epsilon_0 V_s}{V_{dra} + V_s} \quad (1)$$

Table 1. Optimized dimensions of the proposed antenna.

Parameter	Dimension_(mm)	Parameter	Dimension (mm)	Parameter	Dimension_ (mm)
LS = Ws	25	W _g	20	st2	2
L _g	9.4	wdr1	7	lt1	5.4
ldr1	5	wdr2	6	lt2	7.6
ldr2	8	wf1	2	lt3	10.2
lf1	5.9	wf2	1.1	tdr1	4
lf2	7.9	st1	6	tdr2	8

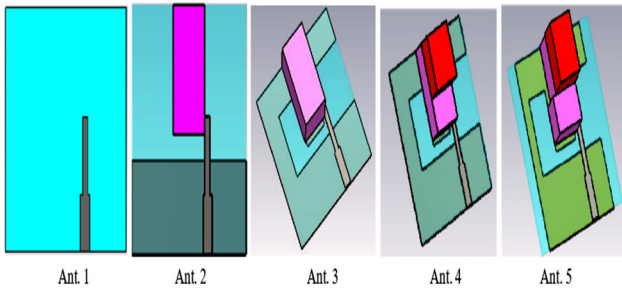


Figure 2. Step evolution of the proposed antenna.

$$Q = \frac{1 + 3\left(\frac{\pi}{\sqrt{\epsilon_{DR}}}\right)^2}{\left(\frac{\pi}{\sqrt{\epsilon_{DR}}}\right)^3 \left[1 + \left(\frac{\pi}{\sqrt{\epsilon_{DR}}}\right)^2\right]} \quad (2)$$

$$Qp = \frac{1 + 3\left(\frac{\pi}{\sqrt{\epsilon_{reff}}}\right)^2}{\left(\frac{\pi}{\sqrt{\epsilon_{reff}}}\right)^3 \left[1 + \left(\frac{\pi}{\sqrt{\epsilon_{reff}}}\right)^2\right]} \quad (3)$$

The total size of DRA is 13 mm × 7 mm × 8 mm. Firstly, the DRA key parameters are calculated using eq. (4), k_x, k_y, k_z, k₀, and resonant frequency values are 448.79, 392.69, 196.34, 230.79 and 10.65 GHz. Similarly, DR1 & DR2 resonant frequencies are 12.7 & 10.02 GHz. The simulated resonant frequency of DRA is 11.28 GHz.

$$f_{TE_{inm}} = \frac{v}{2\pi\sqrt{\epsilon_{reff}}} \sqrt{k_x^2 + k_y^2 + k_z^2} \quad (4)$$

$$k_x = \frac{l\pi}{l_{eff}}, k_y = \frac{n\pi}{w_{eff}}, k_z \tan\left(k_z \frac{h_{DR}}{2}\right) = \sqrt{(\epsilon_{reff} - 1)k_0^2 - k_z^2} \quad (5)$$

$$l_{eff} = l_{dr1} + l_{dr2} \text{ and } w_{eff} = w_{dr1} + w_{dr2} \quad (6)$$

where k₀ represents wave number in the free space, k_x, k_y, and k_z are wavenumbers.

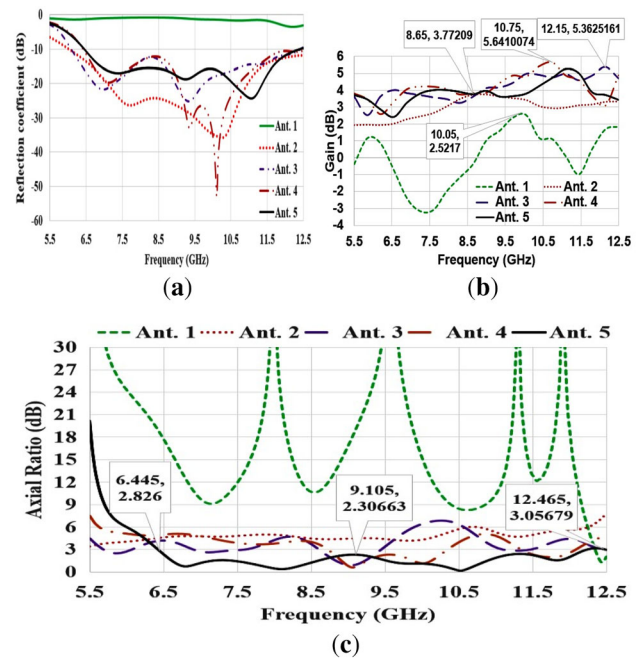


Figure 3. Frequency response concerning (a) Reflection coefficient, (b) Gain and (c) Axial Ratio.

2.3 Field modes and CP mechanism

The simulated E-field vector configuration has been analyzed by field rotation inside the proposed asymmetric DR at the different frequencies. The concept of E-field analysis is reported in [3, 6, 12, 17]. Eq. (1), (4)–(6) are used to calculate TE₁₁₁ fundamental as well as the dominant mode of the antenna. Figure 5 shows the impedance matching of the antenna with the resonant frequencies of the different operating modes. There are two peaks in the real part of the impedance plot in the antenna’s passband, confirming the antenna’s operation with two resonating modes at frequencies 9.1 and 11.28 GHz. Figure 6 shows the E-field distribution inside the DR at 9.1 and 11.28 GHz [17, 19–22]. Figures 6(a)–(b) confirm the operation of an antenna with the fundamental and third-order mode, i.e., TE_{δ11} and TE_{δ13} at frequency 9.1 and 11.28 GHz, respectively. For understanding the mechanism of CP generation,

Table 2. Performance of all five antennas.

Antenna	10 dB impedance BW%	Peak gain (dB)	AR BW (≤ 3)	
			Band 1	Band 2
Ant. 1		2.5	–	
Ant. 2	70.3% (6 to 12.5 GHz)	3.77	–	
Ant. 3	68.1% (6 to 12.4 GHz)	5.64	8.3% (6.9 to 7.5 GHz)	8.9% (8.6 to 9.4 GHz)
Ant. 4	63.8% (6.4 to 12.4 GHz)	5.36	17.3% (8.7 to 10.3 GHz)	
Ant. 5	63.8% (6.5 to 12.4 GHz)	5.6	63.8% (6.5 to 12.4 GHz)	

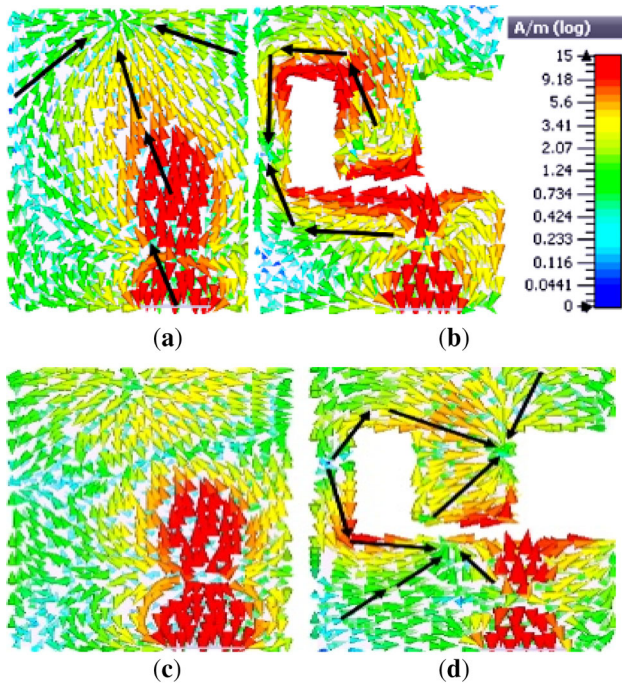


Figure 4. Surface current distribution on the full ground and modified ground; **a–b** 7.2 GHz, **c–d** 9 GHz.

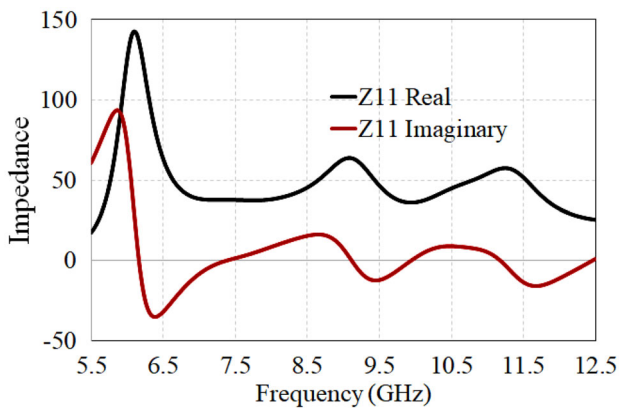


Figure 5. The impedance plot of the antenna.

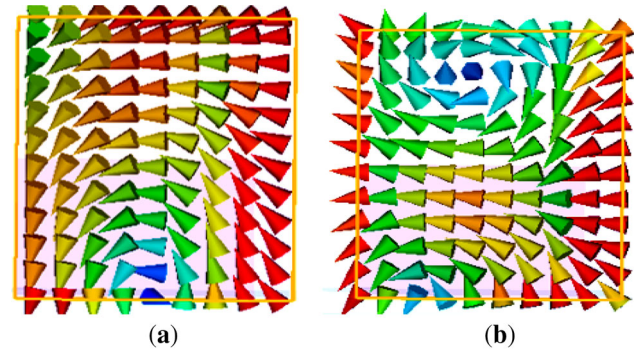


Figure 6. The E -field distribution at **(a)** 9.1 and **(b)** 11.28 GHz.

the E -field distribution is also analyzed in the constant $z = h$ plane at different time instants, shown in figures 7(a)–(d). The rotation of the field vector in the clockwise direction represents the dominant left-hand CP field radiation that could be verified with the radiation pattern analysis (figure 15) reported in the later section of this manuscript. The E -field distribution in the constant z -plane is stated at the

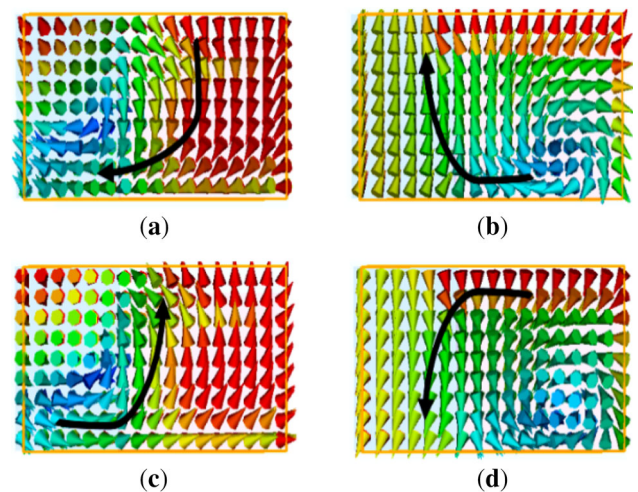


Figure 7. The E -field distribution in constant $z = h$ plane at frequency 9.1 GHz at the time **(a)** $t = 0$, **(b)** $t = T/4$, **(c)** $t = T/2$ and **(d)** $t = 3T/4$.

first-order mode frequency. However, the analysis also represents the clockwise rotation of the field vectors at the higher-order mode frequency. The E-field distribution and the radiation mechanism of the proposed CPDRA are reported broad AR bandwidth [22–24].

3. Parametric study

The parametric study has been performed to obtain optimum dimensions for achieving the best results of the DRA and for which parameter to give the CP inside the antenna structure.

3.1 Variation of the height of DR

The effect of DR heights as t_{dr1} and t_{dr2} are varied, and it observed from figures 8 (a)–(d) that the best values are $t_{dr1} = 4$ mm and $t_{dr2} = 8$ mm for widen impedance bandwidth and AR bandwidth, respectively.

3.2 Variation parameter in F-shaped strip

The F shaped strip with main key parameters are s_{t1} , s_{t2} , l_{t1} , l_{t2} , and l_{t3} . The best values are chosen through optimization as in figures 9 (a–b) on $s_{t1} = 6$ mm (– 3 to 3) and figure 9 (c–d) on $s_{t2} = 2$ mm (– 10 to – 8).

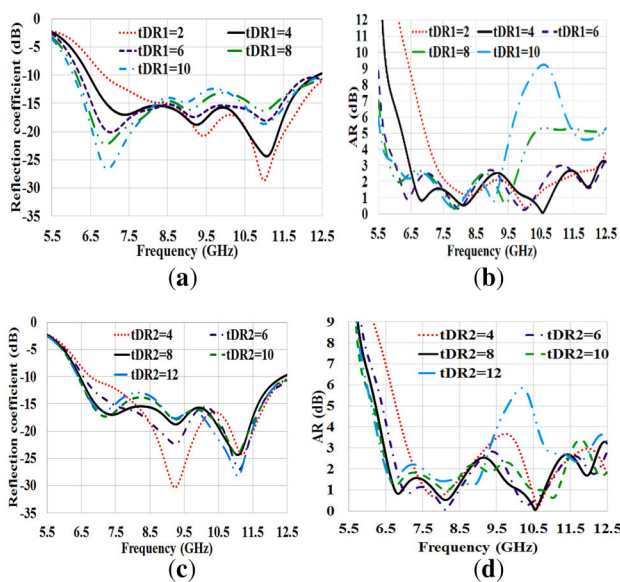


Figure 8. Reflection coefficient and Axial Ratio for various height ($tDR1$ (a and b) and $tDR2$ (c and d)) of DR.

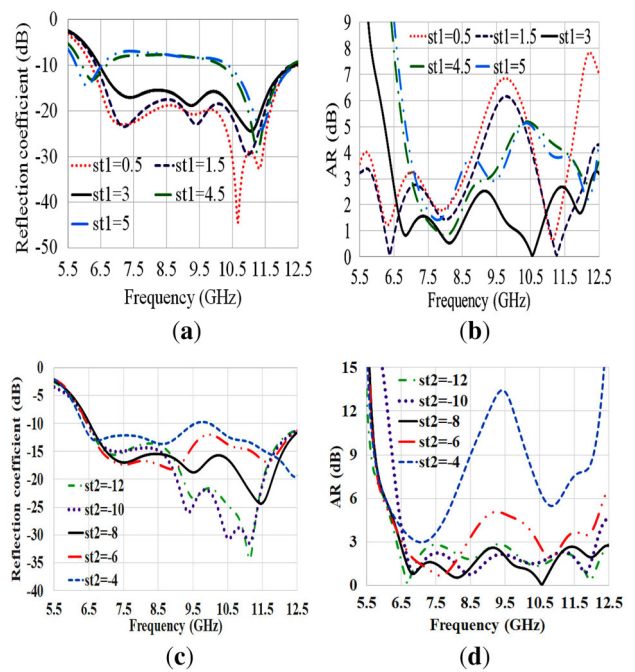


Figure 9. Reflection coefficient and Axial Ratio for varies $st1$ (a–b), and $st2$ (c–d).

3.3 Variation of the partial ground (L_g)

The proposed DRA has with or without an F-shaped metallic strip in the partial ground to achieve the UWB range. Variation in the L_g parameter is shown in figure 10, and the best value of $L_g = 9.4$ mm (– 12.5 to – 3.1) is chosen.

The proposed compact DRA is compared with other literature-reported structures related to parameters such as antenna size, peak gain, impedance bandwidth and AR bandwidth for ultra-wideband operation, as shown in Table 3.

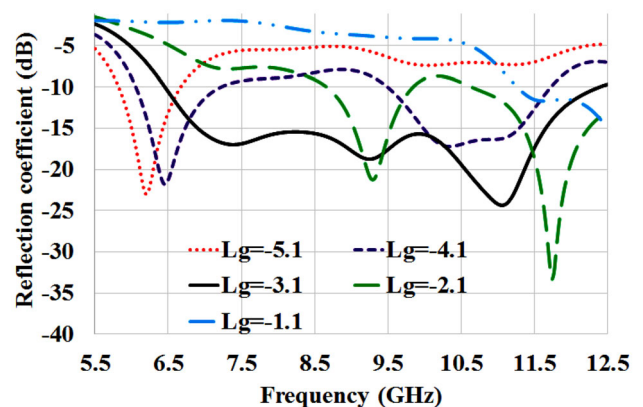


Figure 10. Reflection coefficient with varies L_g .

Table 3. Comparison of CP DRA.

Ref.	Frequency range (GHz)	AR frequency range (GHz)	AR bandwidth (%)	Gain (dB/dBi)	Antenna size
[17]	4.19 to 8.34 GHz	4.17 to 8.32	66.45	2.67 dBic	80 × 80
[18]	4 to 10.5	5.3 to 7	27	4.2 dB	24 × 20
[20]	5.18 to 5.62	5.2 to 5.68	8.82	4.6 dB	44 × 45
[21]	4.24 to 6.57 GHz	4.29 to 6.72 GHz	44.14	2.1 dBi	80 × 80
[26]	7.32–7.68 GHz and 8.34–9.44 GHz	7.43–7.55 GHz and 8.53–8.68 GHz	1.6 and 1.7	3.69 dBi	50 × 50
Proposed antenna	6.4 to 12.4 GHz (simulated) 5.9 to 11.8 GHz (measured)	6.47 to 12.3 GHz (simulated) 5.8 to 6.1 GHz and 6.9 to 10.9 GHz (measured)	62.087 (simulated) 2.52 and 43.73 (measured)	5.6 dB at 11 GHz (measured) 6.01 dB at 11.5 GHz (simulated)	25 × 25

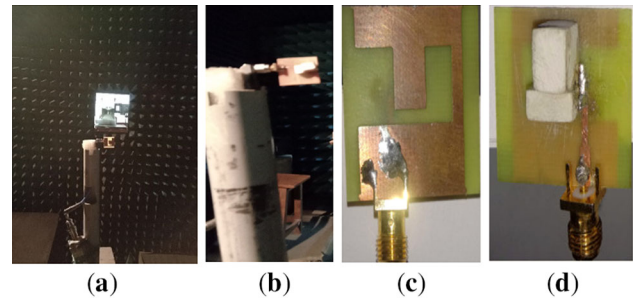


Figure 11. (a–b) Measurement setup back and Front view of DRA (c–d) Back and front view of fabricated DRA.

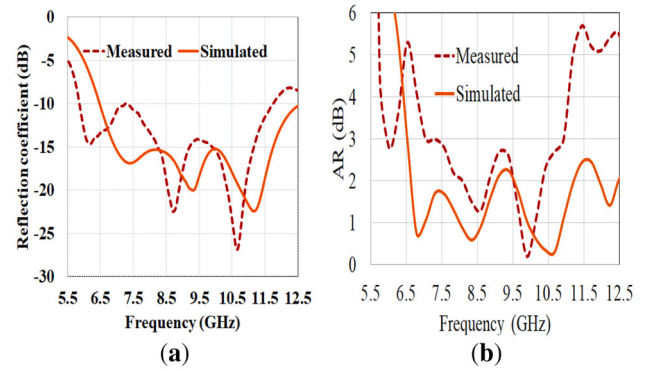


Figure 12. Simulated and measured; (a) S_{11} and (b) AR w.r.t frequency.

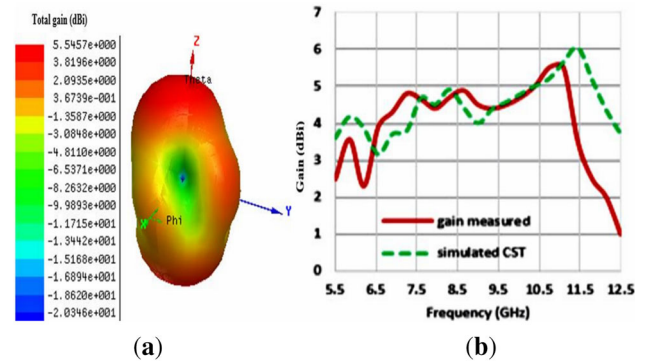


Figure 13. (a) 3-D simulated gain plot at 11 GHz and (b) Gain w.r.t frequency.

4. Results and discussions

The fabricated prototype with testing and measurement setup is shown in figures 11 (a–b), and the fabricated DRA view is shown in figures 11 (c–d). The simulated and measured S_{11} plot and AR plot of the designed antenna are presented in figures 12 (a–b). The measured S_{11} is almost similar to the simulated ones. A slight left-shifting of the three resonance frequencies is observed due to the fastitave epoxy adhesive, which is used to join the DR layers on the

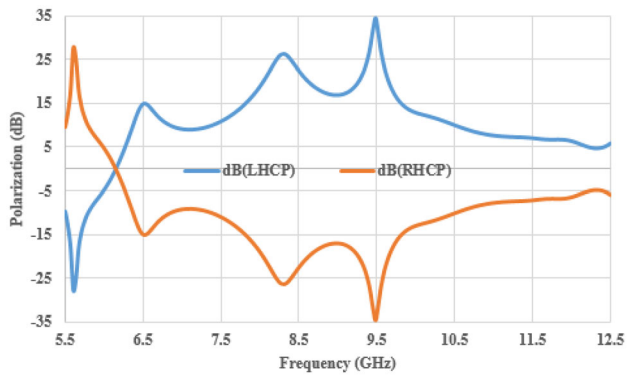


Figure 14. Polarization (dB) of the proposed antenna as LHCP and RHCP with respect to frequency.

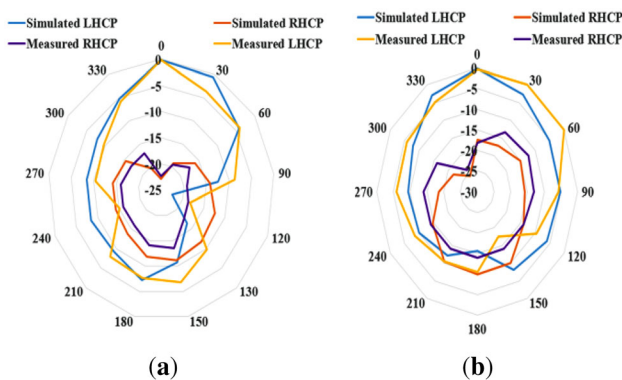


Figure 15. Radiation pattern (a) LHCP and RHCP at 6.6 GHz, (b) LHCP and RHCP at 9.1 GHz.

substrate. Simulated and measured impedance bandwidths of 63.8% (6.4 to 12.4 GHz) and 66.7% (5.9 to 11.8 GHz) have been reported at a central frequency of 9.35 GHz and 8.85 GHz, respectively. Subsequently, from figure 12b, the simulated AR bandwidth is obtained 63.8% (6.47 to 12.3 GHz) and measured are 2.52% and 43.7% (5.8 to 6.1 GHz and 6.9 to 10.9 GHz).

Figure 13(a) shows the simulated gain at 11 GHz. The simulated and measured gain are shown in figure 13b. The antenna's simulated peak gain is 6.01dBi at 11.5 GHz, while the measured peak gain is 5.6 dBi at 11 GHz, according to the figure 13(b).

This proposed antenna is dominated by the left-handed polarization compared to the right-handed polarization, as shown in figure 14. Figures 15(a–b) showed the measured and simulated radiation patterns of the proposed antenna at 6.6 and 9.1 GHz for XZ and YZ planes. A good agreement reported between simulated and measured results. Referring to figures 15(a–b), it is observed that the LHCP fields are much stronger in comparison to the RHCP for CP DRA.

5. Conclusion

A compact asymmetric structured DR is designed and fabricated for CP UWB applications. The antenna is used for two DR blocks with asymmetric height using QWT feeding and an F-shaped metallic strip in the ground plane to obtain simulated AR bandwidth of 63.8% and measured AR bandwidth of 43.7% in the frequency range from 6.4 to 12.4 GHz for circularly polarized DRA. These attractive performances make the present design suitable for UWB operations. This antenna can be used for (C and X band) multiple applications like military applications, satellite communication, weather forecasting, and defense tracking system.

Acknowledgements

The authors are thankful to Prof. M V Kartikeyan, IIT Roorkee, India and Dr. Gaurav Varshney, NIT Patna, India, for providing their support in antenna measurement.

References

- [1] Yazdandoost K Y and Kohno R 2004 Ultra wideband antenna. *IEEE Commun. Mag.* 42(6): S29–32
- [2] Luk K M and Leung K W 2003 *Dielectric resonator antennas handbook*. Hertfordshire: Baldock: 18–20
- [3] Yaduvanshi R S and Parthasarathy H 2016 *Rectangular dielectric resonator antennas*. Springer, New Delhi, India: 1–5
- [4] Ryu K S and Kishk A A 2011 UWB dielectric resonator antenna having consistent omnidirectional pattern and low cross-polarization characteristics. *IEEE Trans. Antennas Propag.* 59(4): 1403–1408
- [5] Abedian M, Rahim S K A and Khalily M 2012 Two-segment compact dielectric resonator antenna for UWB application. *IEEE Antennas Wirel. Propag. Lett.* 11: 1533–1536
- [6] Denidni T A and Weng Z 2011 Hybrid ultrawideband dielectric resonator antenna and band-notched designs. *IET Microwaves Antennas Propag.* 5(4): 450–458
- [7] Yang J and Kishk A 2012 A novel low-profile compact directional ultra-wideband antenna: The self-grounded Bow-Tie antenna. *IEEE Trans. Antennas Propag.* 60(3): 1214–1220
- [8] Majeed A H, Abdullah A S, Sayidmarie K H, Abd-Alhameed R A, Elmegri F and Noras J M 2015 Balanced dual-segment cylindrical dielectric resonator antennas for ultra-wideband applications. *IET Microwaves Antennas Propag.* 9(13): 1478–1486
- [9] Guha D and Kumar C 2016 Microstrip patch versus dielectric resonator antenna bearing all commonly used feeds: An experimental study to choose the right element. *IEEE Antennas Propag. Mag.* 58(1): 45–55
- [10] Petosa A M, Ittipiboon A, Antar Y M, Roscoe D and Cuhaci M 1998 Recent advances in dielectric-resonator antenna technology. *IEEE Antennas Propag. Mag.* 40(3): 35–48

- [11] Pan Y and Leung K W 2010 Wideband circularly polarized trapezoidal dielectric resonator antenna. *IEEE Antennas Wirel. Propag. Lett.* 9: 588–591
- [12] Fakhte S, Oraizi H, Karimian R and Fakhte R 2015 A new wideband circularly polarized stair-shaped dielectric resonator antenna. *IEEE Trans. Antennas Propag.* 63(4): 1828–1832
- [13] Wang K X and Wong H 2015 A circularly polarized antenna by using rotated-stair dielectric resonator. *IEEE Antennas Wirel. Propag. Lett.* 14: 787–790
- [14] Pan Y M and Leung K W 2012 Wideband omnidirectional circularly polarized dielectric resonator antenna with parasitic strips. *IEEE Trans. Antennas Propag.* 60(6): 2992–2997
- [15] Huang C Y, Wu J Y and Wong K L 1999 Cross-slot-coupled microstrip antenna and dielectric resonator antenna for circular polarization. *IEEE Trans. Antennas Propag.* 47(4): 605–609
- [16] Khalily M, Kamarudin M R, Mokayef M, Danesh S and Ghahferokhi S E 2014 A new wideband circularly polarized dielectric resonator antenna. *Radioengineering.* 23(1): 175–180
- [17] Varshney G, Pandey V S and Yaduvanshi R S 2018 Axial ratio bandwidth enhancement of a circularly polarized rectangular dielectric resonator antenna. *Int. J. Microw. Wirel. Technol.* 10(8): 933–941
- [18] Haraz O M and Sebak A R 2010 A novel circularly polarized dielectric resonator antenna for UWB applications. *IEEE Int. Symp. Antennas Propag. CNC-USNC/URSI Radio Sci. Meet. Lead. Wave, AP-S/URSI 2010:* 1–4
- [19] Kumar R and Chaudhary R K 2018 Investigation of higher order modes excitation through F-shaped slot in rectangular dielectric resonator antenna for wideband circular polarization with broadside radiation characteristics. *Int. J. RF Microw. Comput. Eng.* 28(6): 1–11
- [20] Kumari R and Gangwar R K 2018 Circularly polarized slot-coupled square dielectric resonator antenna for WLAN applications. *Microw. Opt. Technol. Lett.* 60(11): 2787–2794
- [21] Varshney G, Pandey V S, Yaduvanshi R S and Kumar L 2017 Wide band circularly polarized dielectric resonator antenna with stair-shaped slot excitation. *IEEE Trans. Antennas Propag.* 65(3): 1380–1383
- [22] Gotra S, Varshney G, Yaduvanshi R S and Pandey V S 2019 Dual-band circular polarisation generation technique with the miniaturisation of a rectangular dielectric resonator antenna. *IET Microwaves Antennas Propag.* 13(10): 1742–1748
- [23] Varshney G 2020 Gain and bandwidth enhancement of a singly fed circularly polarized dielectric resonator antenna. *IET Microwaves Antennas Propag.* 14(12): 1323–1330
- [24] Kumar R, Varshney G, Yaduvanshi R S, Kumar D and Pandey V S 2020 Dual-band dielectric resonator antenna with multi-frequency circular polarization. *IET Microwaves, Antennas Propag.* 14(5): 435–439
- [25] Jehle M, Maurice R, David S, Erich M and Daniel N Estimation of ionospheric TEC and Faraday rotation for L-band SAR. In: *International Society for Optics and Photonics.* 5979: 59790U
- [26] Dash S K, Khan T and Kanaujia B K 2018 Circularly polarized dual facet spiral fed compact triangular dielectric resonator antenna for sensing applications. *IEEE Sens. Lett.* 2(1): 1–4